Chemical Engineering Journal 464 (2023) 142687

Contents lists available at ScienceDirect

Chemical Engineering Journal

journal homepage: www.elsevier.com/locate/cej

A two-pronged detection of atherosclerosis with a dual-channel fluorescent probe for viscosity and hypochlorous acid

Zhenkai Wang [a,b,e,1], Shan Wang [c,1], Bingya Wang [a], Jianliang Shen [a], Linlu Zhao [b,e,*], Fabiao Yu [b,e,*], Ji-Ting Hou [a,d,*]

[a] National Engineering Research Center of Ophthalmology and Optometry, Eye Hospital, Wenzhou Medical University, Wenzhou 325027, China
[b] Key Laboratory of Hainan Trauma and Disaster Rescue, The First Affiliated Hospital of Hainan Medical University, Hainan Medical University, Haikou 571199, China
[c] Key Laboratory of Intelligent Treatment and Life Support for Critical Diseases of Zhejiang Province, the First Affiliated Hospital of Wenzhou Medical University, Wenzhou 325000, China
[d] Key Laboratory of Clinical Laboratory Diagnosis and Translational Research of Zhejiang Province, The First Affiliated Hospital of Wenzhou Medical University, Wenzhou 325000, China
[e] Engineering Research Center for Hainan Bio-Smart Materials and Bio-Medical Devices, Key Laboratory of Emergency and Trauma, Ministry of Education, Key Laboratory of Hainan Functional Materials and Molecular Imaging, College of Emergency and Trauma, Hainan Medical University, Haikou 571199, China

ARTICLE INFO

Keywords:
Fluorescent probe
Hypochlorous acid
Viscosity
Near-infrared emission
Atherosclerosis

ABSTRACT

The precise detection of atherosclerosis has been a research hot point since its importance in the diagnosis of cardiovascular diseases. Here we synthesized a near-infrared fluorescent probe **AS-CN** with a D – π – A structure, enabling independent dual-response determination of hypochlorous acid (HOCl) and viscosity during AS progression. The performance of this probe is excellent, with large Stokes shift, low detection limit, high sensitivity, and good biocompatibility. The simultaneous variations of HOCl and viscosity during the formation of foam cells were successfully investigated for the first time. Especially, we further applied it to achieve the non-invasive *in vivo* detection in the atherosclerotic mouse and realized the evaluation of atherosclerosis from chemical (ROS) and physical (viscosity) dimensions, respectively. We hope that **AS-CN** acts as a potent tool in the detection of atherosclerosis.

1. Introduction

According to the latest survey report, 523 million people worldwide suffered from cardiovascular diseases (CVDs). Even more alarming is that about 18.6 million of them have been threatened with death, which accounts for one-third of the total number of deaths in the world [1–3]. Atherosclerosis (AS) is one of the most common CVDs and even a key contributing factor to many diseases of other systems, such as peripheral arterial disease, coronary artery disease, cerebrovascular diseases, neurodegenerative diseases, et al. [2,4,5]. It is worth noting that the progression of the lesion can reduce blood flow in the lumen by more than 50%, and even when the plaque sloughs off it can also lead to a variety of fatal symptoms including myocardial infarction and stroke [6]. Therefore, efficient treatment of AS is of great significance. The imaging methods currently available for clinical diagnosis of AS mainly include magnetic resonance imaging (MRI), computed tomography (CT), and ultrasound (US), but these methods only provide anatomical and physiological information. This makes AS undetectable until qualitative lesions in the arterial lumen are observed. In contrast, detection of AS at its early stage can contribute to a timely intervention and improve the treatment efficiency. Therefore, novel detection tools for precise detection of AS at the early stage are urgently demanded [4,7], albeit a big challenge.

The pathogenesis of atherosclerosis is mainly related to persistent inflammation and increased dyslipidemia [5]. Among them, the oxidation of low-density lipoprotein cholesterol (LDL-c) is considered to be one of the most important leading causes in the occurrence and development of AS [8–10]. When the concentration of LDL-c is continuously

* Corresponding authors at: Key Laboratory of Hainan Trauma and Disaster Rescue, The First Affiliated Hospital of Hainan Medical University, Hainan Medical University, Haikou 571199, China (L. Zhao, F. Yu); National Engineering Research Center of Ophthalmology and Optometry, Eye Hospital, Wenzhou Medical University, Wenzhou 325027, China (J.-T. Hou).
E-mail addresses: zhaolinlu@hainmc.edu.cn (L. Zhao), yufabiao@hainmc.edu.cn (F. Yu), houjiting2206@163.com (J.-T. Hou).
[1] These authors contributed equally to this work.

https://doi.org/10.1016/j.cej.2023.142687
Received 27 February 2023; Received in revised form 21 March 2023; Accepted 27 March 2023
Available online 29 March 2023

higher than the physiological level, LDL accumulates in the arterial intima, and the LDL infiltrating the intima is converted into oxidized low-density lipoprotein (ox-LDL) through oxidative modification, which is further processed by macrophages or epithelial phagocytosis to form foam cells, an indicator of early AS lesion [2,11,12]. The resulting foam cells accumulate in the intima of the blood vessel, and their migration is inhibited, thereby generating the lipid-rich center (necrotic core) of the atherosclerotic plaque by binding to cholesterol and necrotic cell debris [8,13–15]. It is worth mentioning that recent studies have shown that AS may also be a mitochondrial disease and mitochondrial dysfunctions are regarded as one of the primary factors contributing to the formation of foam cells [16,17]. Especially, mitochondria have emerged as a potential therapeutic target for AS [17]. Therefore, developing precise and sensitive tools to detect mitochondrial dysfunctions should aid in the diagnosis and mitochondria-targeted therapy for AS.

Owing to its non-invasive, real-time and high-resolution imaging ability, fluorescence imaging has become a powerful tool in biomedical imaging [18–24], and a hand of fluorescence sensors for AS imaging has been presented [25–32]. However, most of these probes were used to monitor AS symptoms through targeting lipid droplets [27–30], and quite a few of them were applied for *in vivo* imaging due to the short emission wavelength. In addition, compared with sensors for single analyte, those for two or more analytes can provide more information about AS pathology, and improve the diagnosis precision [33]. Recently, Tang group reported the first fluorescent sensor based on MOFs that could simultaneously detect two analytes (pH and phosphate) during AS progression, while its *in vivo* imaging was not still realized [26]. Accordingly, it is necessary yet challenging to develop a fluorescent probe that can respond to multiple targets in mitochondria with dia-critical emission wavelengths and the probe will be extremely preferable if it is applicable to *in vivo* imaging. AS occurrence is tightly associated with inflammation [5]. Along with the initiation of inflammation, an oxidative stress in mitochondria is usually accompanied, leading to upregulated level of reactive oxygen species (ROS) [16]. Meanwhile, mitochondrial viscosity has been confirmed to be elevated under inflammatory stimulation [34]. Therefore, during AS formation, both chemical (ROS) and physical viscosity changes are expected. As a result, a fluorescent probe that can simultaneously monitor ROS and viscosity changes in mitochondria should be of great potential for precise assessment of AS progression from chemical and physical dimensions since it will provide more comprehensive and informative knowledge about AS pathogenesis.

2. Experimental section

2.1. Synthesis of probe *AS-CN*

The synthesis and characterization of the probe **AS-CN** was outlined in Scheme S1. The Suzuki coupling reaction between *p*-bromophenylacetonitrile and pyridine-4-boronic acid over a palladium salt catalyst gave the initial intermediate 1 in a yield of 88%. Next 1 and 2 were condensed under KOH condition to afford another intermediate compound 3 with a yield of 95%. Finally 3 (108 mg, 0.25 mmol) and ethyl iodide (44 μL, 0.55 mmol) were dissolved in 3 mL of anhydrous CH_3CN. The mixture was heated to reflux at 85 °C for 13 h. The reaction was monitored by TLC. After the reaction was completed, the solvent was evaporated. The crude product was subjected to column chromatography using dichloromethane/MeOH = 50:1 (v/v) as the eluent, and probe **AS-CN** was obtained as a deep-red powdery solid (145 mg, yield: 98%). ^{1}H NMR (600 MHz, DMSO-d_6), δ 9.15 (d, J = 7.1 Hz, 2H), 8.59 (d, J = 7.1 Hz, 2H), 8.24 (d, J = 8.7 Hz, 2H), 8.13 (s, 1H), 7.98 (d, J = 8.6 Hz, 2H), 7.90 (dd, J = 8.9, 2.2 Hz, 1H), 7.79 (d, J = 2.1 Hz, 1H), 7.23 (ddd, J = 8.3, 7.3, 1.6 Hz, 1H), 7.20 – 7.15 (m, 2H), 7.08 (dd, J = 8.3, 1.1 Hz, 1H), 6.99 (td, J = 7.5, 1.1 Hz, 1H), 4.64 (q, J = 7.3 Hz, 2H), 4.00 (q, J = 7.0 Hz, 2H), 1.58 (t, J = 7.3 Hz, 3H), 1.34 (t, J = 6.9 Hz, 3H); ^{13}C NMR (150 MHz, DMSO-d_6), δ 153.93, 147.19, 145.15, 143.58, 143.28, 138.08, 133.85, 130.48, 129.45, 128.55, 128.27, 128.03, 127.68, 126.97, 124.91, 123.82, 123.05, 122.04, 118.58, 116.39, 115.83, 106.10, 56.08, 42.11, 16.84, 12.99. HRMS (ESI): m/z 460.1842; $[M]^+$ found: 460.1863.

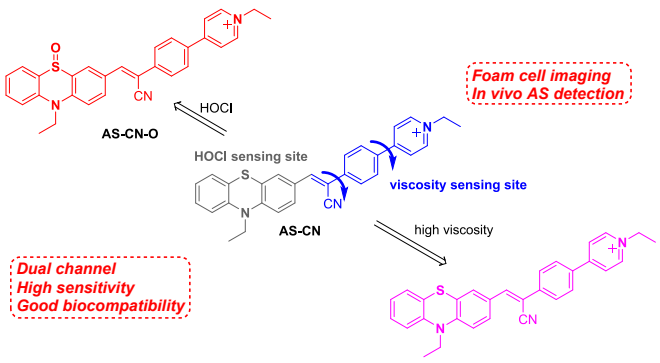

Scheme 1. Design strategy of probe **AS-CN** and its schematic response mechanism to HOCl and viscosity.

2.2. Establishment of AS mouse models

The 8-week-old apolipoprotein E-deficient (ApoE-/-) mice for atherosclerosis are fed with a high-fat diet for 12 weeks, and C57BL/6 mice of the same sex and age were used as controls. We performed right carotid artery ligation in mice after 10 weeks of high-fat diet feeding to increase the inflammation of the right carotid artery. After 2 weeks, the mice were injected with the probe **AS-CN** through the tail vein, and imaged by a small animal *in vivo* imaging system after 60 min. After 8 weeks of $ApoE^{-/-}$ mice on a high cholesterol diet, colchicine treatment (0.25 mg/kg body weight) was started once daily for more than four weeks, then imaged the bilateral carotid arteries of mice using **AS-CN**.

3. Results and discussion

3.1. Design of probe *AS-CN*

Our group for the first time suggested that excessive HOCl is definitely produced in mitochondria along with the AS progression in macrophages using a fluorescent probe **AS-ClO** [32]. However, its emission wavelength located around 520 nm is too short for *in vivo* imaging. To solve this obstacle, we strive to modify a new desirable probe for the simultaneous *in vivo* detection of HOCl and viscosity. Phenothiazine (PTZ) unit is retained as it is an excellent responsive site for HOCl [35]. A molecular rotor 4-(4-(1-cyanovinyl)phenyl)-1-methylpyridinium (CPP) is introduced to the 3-position of PTZ to enable the probe with viscosity sensing performance [36]. The crucial pyridinium moiety can not only improve the water solubility of **AS-CN**, but also deliver the probe to mitochondria owing to its inherent positive charge. A strong intramolecular charge transfer (ICT) photophysical process from PTZ to pyridinium is expected to facilitate a near-infrared (NIR) emission of the probe under viscous condition, and the cyano group will amplify the ICT effect. Meanwhile, under HOCl oxidation, **AS-CN** is converted into **AS-CN-O**, which shows a blue-shifted yet red emission, thus realizing the discriminative detection of HOCl and viscosity *in vitro* and *in vivo* (Scheme 1).

3.2. Spectroscopic properties

The spectral responses of **AS-CN** in different solvents were investigated, including methanol, ethanol, acetonitrile, dichloromethane, *N*, *N*-dimethylformamide, $CHCl_3$, acetone, and glycerol. As shown in Fig. 1A, the probe showed negligible emission in the range of 480–850 nm in solvents with different polarity, while an obvious emission band around

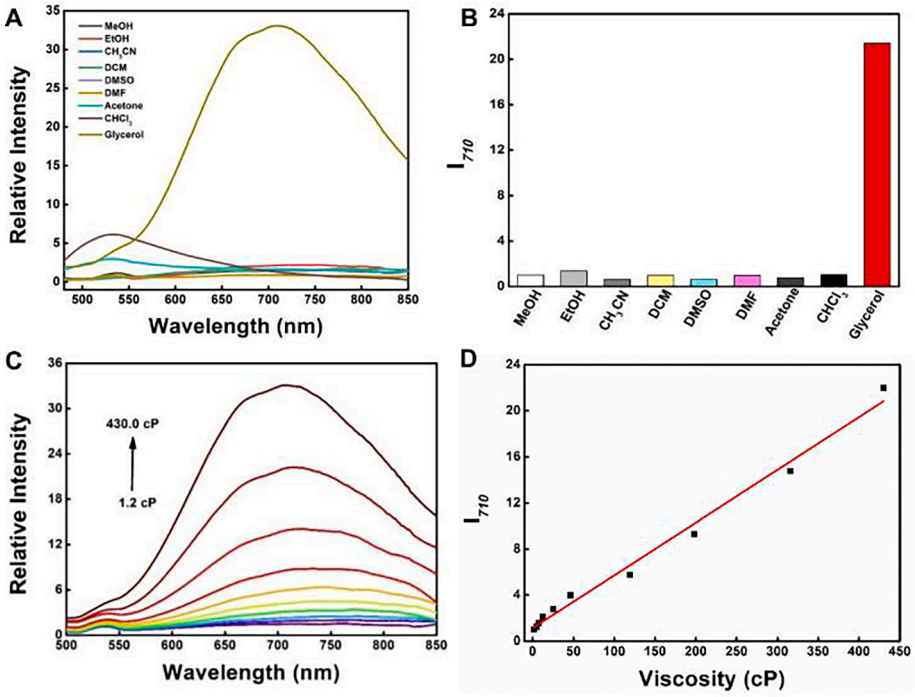

Fig. 1. Optical response of **AS-CN** to viscosity. (A) Fluorescence spectra of **AS-CN** (10 μM) in different organic solvents. (B) Fluorescence intensity of **AS-CN** at 710 nm in different organic solvents. (C) Fluorescence spectra of **AS-CN** in MeOH with increasing fractions of glycerol. (D) Linear response between fluorescence intensity I710 and viscosity. λ_{ex} = 460 nm. λ_{em} = 710 nm, slit width: 5 nm/5 nm.

710 nm was observed in glycerol, a highly viscous solvent. Compared with its emission in MeOH, the probe's fluorescence intensity at 710 nm in glycerol increased by 22 times (Fig. 1B). This result suggests that **AS-CN** could serve as a viscosity-sensitive indicator. Furthermore, the optical behaviors of the probe to viscosity were evaluated. Solvents with different viscosity were obtained by mixing increasing fractions of glycerol in MeOH, with viscosity ranging from 1.2 (0% glycerol) to 450 cP (90% glycerol) [37]. As depicted in Fig. 1C and D, the probe barely fluoresced in MeOH, which is due to the non-radiative decay induced by free

intramolecular motion (rotation, vibration, etc.). When the viscosity increased to 25.2 cP, an emission peak around 750 nm appeared. Then, the emission peak hypochromatically shifted to 710 nm along with the elevation of viscosity. Interestingly, the absorption spectra of the probe displayed minute variations to increasing glycerol proportions (Fig. S1), implying that the probe does not aggregate in viscous condition. Therefore, the intensity enhancement of **AS-CN** induced by glycerol is ascribed to the restriction of intramolecular motion in viscous condition

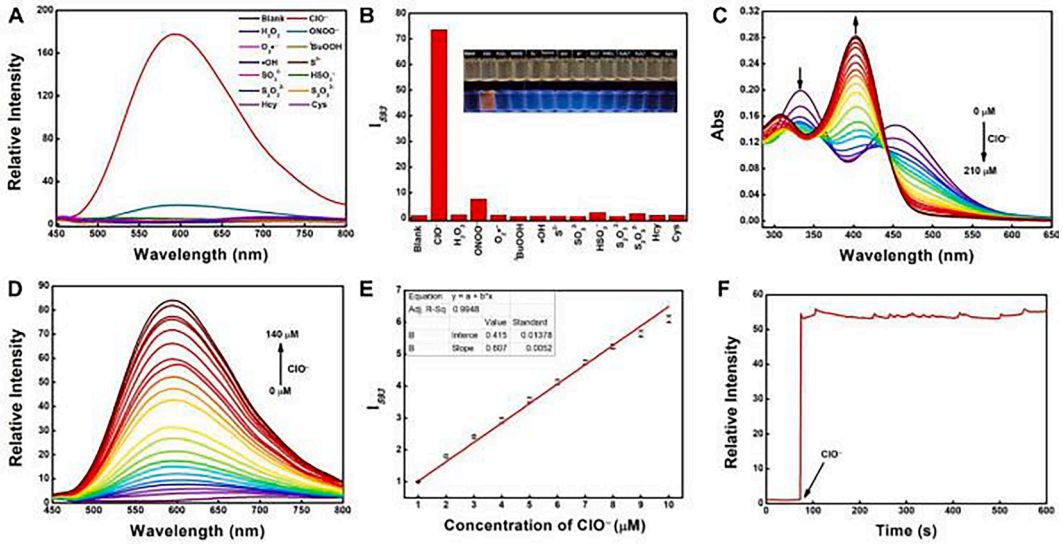

Fig. 2. Optical response of **AS-CN** to HOCl. (A) Fluorescence spectrum of **AS-CN** (10 μM) before and after addition of various reactive species. (PBS, pH 7.2–7.4, 10 mM). (B) The intensity changes of **AS-CN** before and after addition of various reactive species, and the color of the solution after adding different reactive oxygen species and **AS-CN**. (C) UV–vis spectrum of **AS-CN** (10 μM) toward various concentrations of ClO^- in 20% EtOH solution. (PBS, pH 7.2–7.4, 10 mM). (D) Fluorescence of spectra **AS-CN** (10 μM) toward various concentrations of ClO^- in 20% EtOH solution. (PBS, pH 7.2–7.4, 10 mM). (E) Linear relationship between the fluorescence intensity I_{593} of **AS-CN** (10 μM) and the concentrations of ClO^- (1.0–10 μM). (F) Time-dependent kinetic measurement of the fluorescent response to ClO^- (50 μM) of **AS-CN** (10 μM). λ_{ex} = 395 nm, λ_{em} = 593 nm, slit width: 3 nm/3 nm.

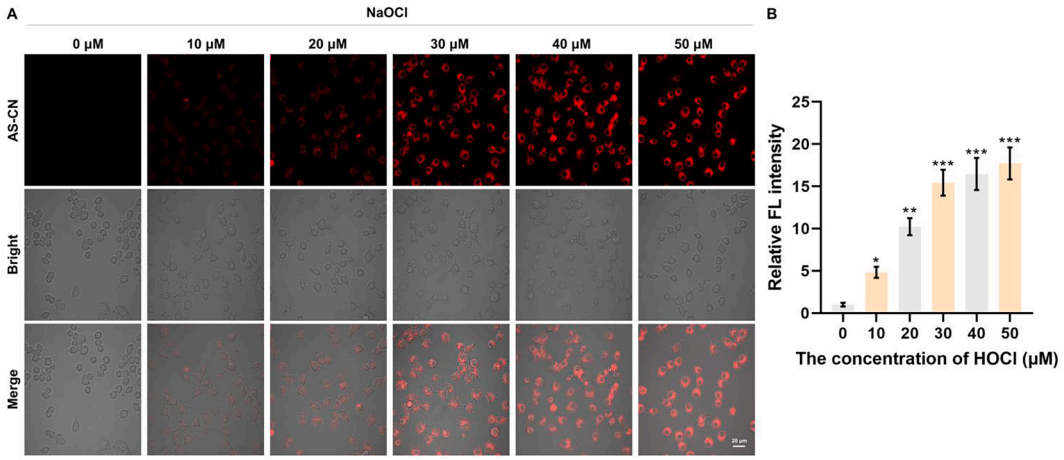

Fig. 3. Response of **AS-CN** to exogenous HOCl in RAW264.7 cells. (A) RAW264.7 cells were treated with 0–50 μm NaOCl for 30 min, then treated with **AS-CN** (10 μM) for 30 min, and imaged under a laser confocal microscope. λ_{ex} = 405 nm, λ_{em} = 500–600 nm. Scale bar: 20 μm. (B) Normalized average fluorescence intensity of **AS-CN**. Data are mean ± SEM. * $p < 0.05$, ** $p < 0.01$, *** $p < 0.001$. Analyzed cells were obtained from three replicates.

rather than the formation of aggregates, although CPP could facilitate aggregation-induced emission [36]. To further validate the importance of CPP unit, the fluorescence spectra of compound 3, an analogue which has no positive charge on pyridine unit, were inspected in different solvents. As shown in Fig. S2, compound 3 emitted faint to bright fluorescence in different solvents with emission peaks ranging from 600 to 630 nm. Especially, its emission intensity in glycerol was weaker than that in most solvents. Therefore, the positive charge of CPP unit is crucial not only for the viscosity sensing performance of **AS-CN**, but also for its NIR emission at 710 nm because of its stronger ICT effect. It should be noted that the viscosity scope tested above covers the viscosity range in cancer cells [38], which is critical for the following bioimaging experiments.

Subsequently, the sensing performance of **AS-CN** to HOCl was measured. First, the absorption spectra of the probe were recorded in the presence of common ROS (H_2O_2, $ONOO^-$, $O_2^{\bullet-}$, ^tBuOOH, •OH, and ClO^-), reactive sulfur species (S^{2-}, SO_3^{2-}, HSO_3^-, $S_2O_3^{2-}$, and $S_2O_5^{2-}$), biothiols (homocysteine (Hcy) and cysteine (Cys)). As shown in Fig. S3, **AS-CN** displayed two main absorbance bands at 335 and 450 nm. When ClO^- was added to the probe solution, the two absorption peaks disappeared, and a new strong absorbance at 400 nm was generated along with a color change from yellowish-brown to light yellow (Fig. 2B),

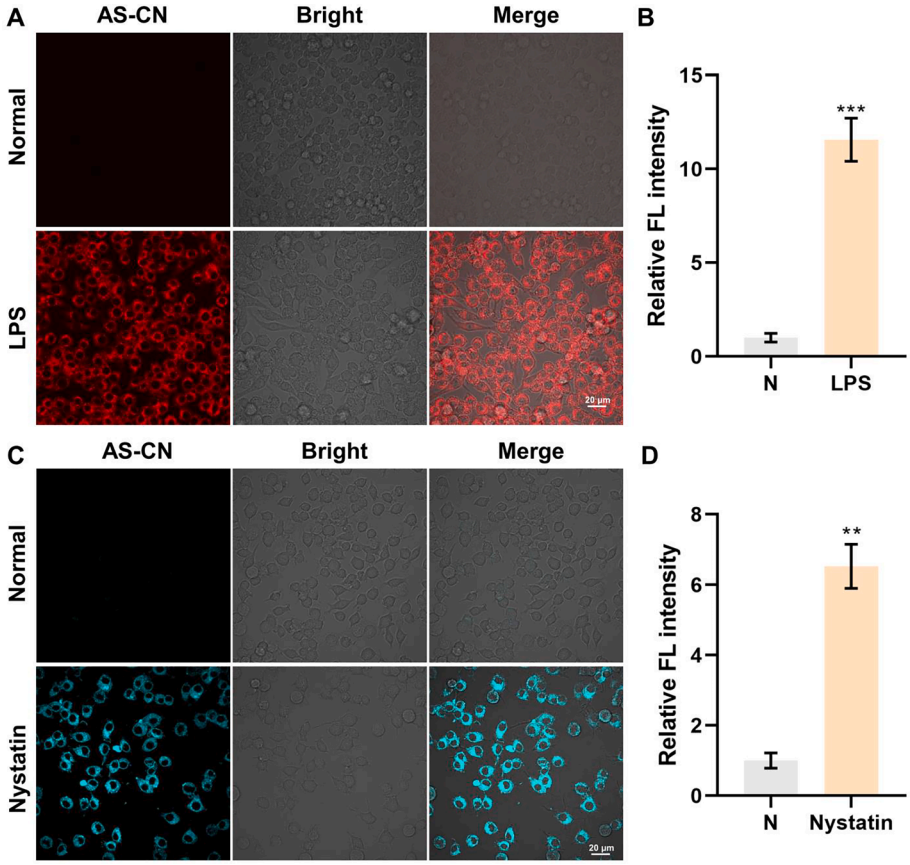

Fig. 4. Response of **AS-CN** to endogenous HOCl and viscosity in RAW264.7 cells, respectively. (A) RAW264.7 cells were treated with LPS (1 μg/ml) for 6 h, then treated with **AS-CN** (10 μM) for 30 min and imaged under a confocal laser. λ_{ex} = 405 nm, λ_{em} = 500–600 nm. (B) Normalized average fluorescence intensity in A. (C) RAW264.7 cells were first treated with nystatin (10 μM) for 6 h, then **AS-CN** (10 μM) for 30 min and imaged by confocal laser. λ_{ex} = 445 nm, λ_{em} = 690–790 nm. (D) Normalized average fluorescence intensity in C. Data are mean ± SEM. ** $p < 0.01$, *** $p < 0.001$. Analyzed cells were obtained from three replicates. Scale bar: 20 μm.

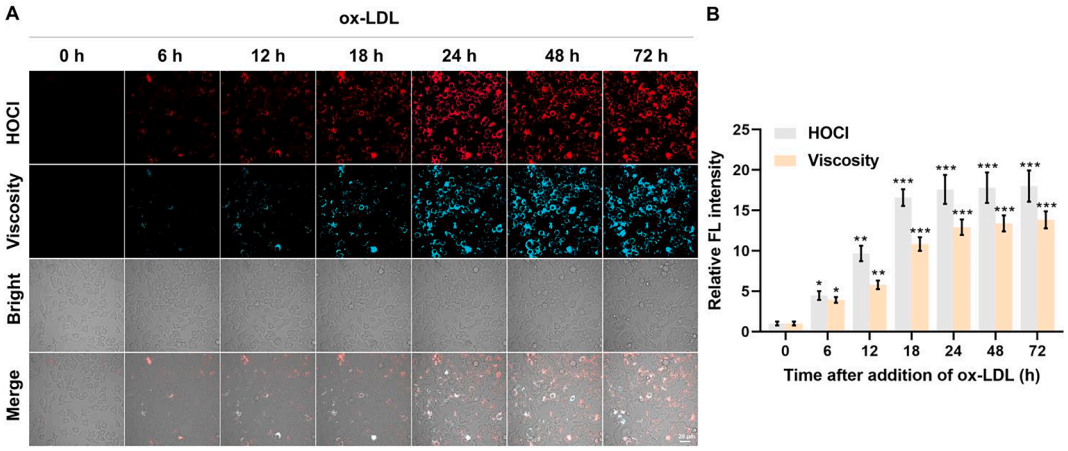

Fig. 5. Fluorescence imaging of changes in HOCl and viscosity levels during foam cell formation by **AS-CN**. (A) The first row: the red fluorescence channel image of HOCl imaging; the second row: the blue fluorescence channel image of viscosity imaging; the third row: cell brightfield image; the fourth row: the three overlay images. (B) Normalized average fluorescence intensity of **AS-CN**. Data are mean ± SEM. * $p < 0.05$, ** $p < 0.01$, *** $p < 0.001$. Analyzed cells were obtained from three replicates. Red channel: λ_{ex} = 405 nm, λ_{em} = 500–600 nm; Blue channel: λ_{ex} = 445 nm, λ_{em} = 690–790 nm. Scale bar: 20 μm.

suggesting a reaction between the probe and ClO^-. By contrast, the addition of the other reactive species caused little changes in the spectra, indicating the high selectivity of the probe to ClO^-. To validate the reaction mechanism between **AS-CN** and HOCl, their reaction mixture was subjected to HRMS analysis. It can be seen that an ion peak at m/z = 476.1802 appeared in the MS spectrum, which is corresponding to **AS-CN-O** (Fig. S4). Therefore, the blue shift of the absorption from 450 to 400 nm was ascribed to the reduced ICT effect by oxidation of PTZ unit, as reported by others [35]. Afterwards, the emission profiles of the probes were also examined. As exhibited in Fig. 2A, the probe emitted no fluorescence in aqueous solution probably due to the potent ICT effect [39]. Upon addition of ClO^-, a 73-fold intensity enhancement at 593 nm was observed, which might be owing to the reduced ICT effect after oxidation of PTZ unit, and the fluorescence color was changed from dark to orange. Other reactive species triggered neglectable spectral variations except that $ONOO^-$ induced a 7-fold increase in the strength. Considering the very short physiological half-life (<10 ms) of $ONOO^-$ [40], we still believe that the probe is highly selective for HOCl. Furthermore, the emission responses of the probe to various metal ions were checked, and no interference was found (Fig. S5). Notably, the emission wavelength of **AS-CN-O** at 593 nm is markedly resolved from that of **AS-CN** in glycerol, which is essential for the dual-channel detection of HOCl and viscosity.

Then the optical response of **AS-CN** toward HOCl was tested in detail. Upon continuous addition of NaOCl, the absorbance bands of the probe at 335 and 450 nm decreased gradually, and a prominent peak at 400 nm was augmented (Fig. 2C). In parallel, the emission intensity at 593 nm was dramatically enhanced and plateaued after 14 equiv. of NaOCl was added (Fig. 2D). A good linearity was calibrated between the intensity at 593 nm and the concentration of HOCl in the range of 1.0–10 μM (R^2 = 0.9948) (Fig. 2E), and a low detection of limit was calculated to be 12 nM accordingly, suggesting a superb sensitivity of the probe. In order to further explore the reaction time between HOCl and the probe, 10 equiv. of HOCl was spiked into the probe solution, and the fluorescence intensity rose sharply within a few seconds, signifying a rapid response of the probe to HOCl (Fig. 2F).

3.3. Intracellular imaging of HOCl and viscosity

After demonstration of the desirable sensing performance of **AS-CN** toward HOCl and viscosity, we intended to utilize the probe for further imaging tests. To verify whether the probe **AS-CN** can be used for biological detection, we selected HeLa cells and RAW 264.7 cells for MTT biotoxicity assessment before bioimaging. After the cells were incubated with the probe for 24 h, their viability remained higher than 80% even when the concentration of the probe reached 100 μM, (Fig. S8), showing that **AS-CN** displays low cytotoxicity. Next, the ability of **AS-CN** to detect exogenous and endogenous HOCl in living cells was investigated. RAW264.7 cells were firstly pretreated with different concentrations of NaOCl (0, 10, 20, 30, 40, 50 μM) for 30 min, and then incubated with the probe (10 μM) for another 30 min. It can be observed that in the emission window of 500–600 nm, neglectable light could be monitored in the cells only treated with probe. Along with the gradual increment of exogenous HOCl concentration, the red fluorescence signal in cells was enhanced stepwise (Fig. 3), suggesting that **AS-CN** can respond sensitively to exogenous HOCl in living cells. Additionally, when RAW264.7 cells were stimulated by lipopolysaccharide (LPS, an inflammation inducer), an obvious elevation of HOCl level was found by virtue of the probe (Fig. 4A), indicating the capability of the probe to measure endogenous HOCl in cells. Similar results were also obtained in HeLa cells (Fig. S9 and S10). Notably, in LPS-treated living cells, bright fluorescence signals can be recorded in every cell, implying superb cell membrane permeability of the probe. Considered in concert, **AS-CN** is quite suitable for monitoring exogenous and endogenous HOCl in different kinds of cells. Subsequently, the optical response of **AS-CN** to intracellular viscosity changes was inspected. Briefly, RAW264.7 cells were pre-treated with nystatin for 6 h before incubation with the probe since nystatin can induce viscosity upregulation in cells [41]. In Fig. 4C, in normal cells, little fluorescence was observed in the emission window of 690–790 nm, suggesting a low-viscosity microenvironment. However, dramatically intensified fluorescence was visualized in nystatin-treated cells, indicating the reinforced intracellular viscosity. The same phenomena were achieved in HeLa cells (Fig. S10). These results showed that **AS-CN** could be used to illustrate viscosity variations in living cells.

According to the above imaging results, we can observe that the fluorescence of the probe mainly centered outside nucleus. Taking into account of the positively charged pyridinium group of **AS-CN**, the probe was speculated to accumulate in mitochondria. Therefore, the localization of **AS-CN** in cells was verified. nystatin-stimulated RAW264.7 cells and HeLa cells were incubated with **AS-CN** and a commercial mitochondrial tracking probe (Mito-Tracker Green, MTG), respectively. As expected, the fluorescence of **AS-CN** and MTG were well overlapped, and their Pearson's correlation coefficients in both cell types were calculated as 0.86 and 0.87, respectively, which indicated that **AS-CN** was primarily localized in mitochondria (Fig. S11).

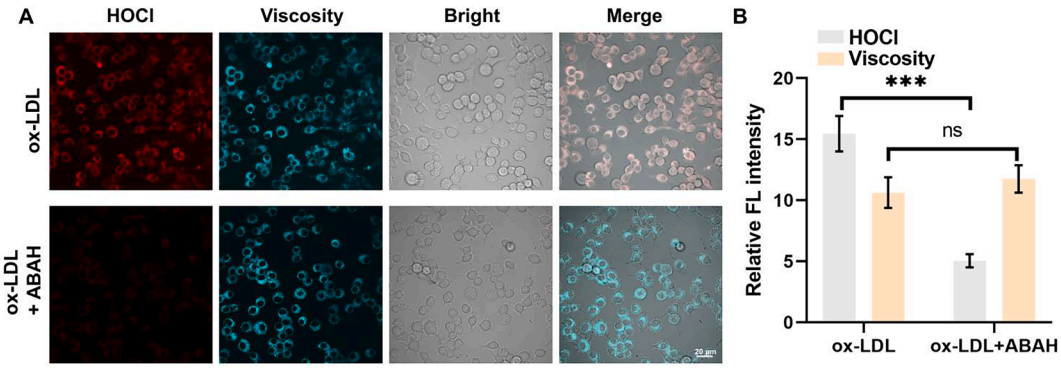

Fig. 6. Verification experiment of dual-channel response of **AS-CN**. (A) The first row: RAW264.7 cells were pretreated with ox-LDL (20 μg/mL) for 18 h, and then treated with **AS-CN** (10 μM) for 30 min; The second row: RAW264.7 cells were pretreated with ABAH (100 μM) for 3 h, then treated with ox-LDL (20 μg/mL) for 18 h, and treated with **AS-CN** (10 μM) for 30 min; (B) Normalized average fluorescence intensity of **AS-CN**. Data are mean ± SEM. *** $p < 0.001$, ns: no statistical significance. Analyzed cells were obtained from three replicates. Red channel: $\lambda_{ex} = 405$ nm, $\lambda_{em} = 500–600$ nm; Blue channel: $\lambda_{ex} = 445$ nm, $\lambda_{em} = 690–790$ nm. Scale bar: 20 μm.

3.4. Imaging HOCl and viscosity in foam cells

After confirming the excellent sensing performance of **AS-CN** toward HOCl and viscosity in separate channels, we aimed to use the probe for AS detection. As reported, a hallmark feature of AS is the appearance of foam cells, which are formed by phagocytosis of lipids by macrophages or smooth muscle cells, accompanied by an inflammatory response [12]. As a result, detection of HOCl and viscosity changes in foam cells is of great potential for diagnosis of early AS. For this purpose, RAW264.7 was firstly treated with ox-LDL to form foam cells and a commercial dye Nile Red was exploited to validate the formation of foam cells. Using the live cell workstation, we continuously photographed the process of phagocytosis of ox-LDL by RAW264.7 cells for 72 h. The results showed that the fluorescence of Nile Red began to increase after adding ox-LDL at the 6th hour, and leveled off within 24 h, identifying the successful construction of foam cells(Fig. S12). Afterwards, ox-LDL-stimulated RAW264.7 cells were cultured with **AS-CN**, and the fluorescence signals from both HOCl and viscosity channels were collected dynamically.

As depicted in Fig. 5, with the prolonging incubation time, fluorescence intensities in both channels were progressively enhanced, and plateaued within 24 h, which is consistent with the formation duration of foam cells. The results showed that during the progression of foam cells, HOCl level and viscosity in mitochondria are concurrently elevated, and these two markers share a consistent development trend.

As noticed in the emission spectra of **AS-CN** in the presence of HOCl, feeble off-peak fluorescence beyond 690 nm was measured, which might induce false positive signal in viscosity channel in the above experiments. In order to get deeper insight of such case, RAW264.7 cells were incubated with 4-aminobenzoic acid hydrazide (ABAH, an inhibitor of MPO enzyme) before ox-LDL treatment. As shown in Fig. 6, ox-LDL-treated cells exhibited strong fluorescence in both HOCl and viscosity channels. In contrast, fluorescence in HOCl channel was apparently attenuated in ABAH-pretreated cells while that in viscosity channel barely varied. The results suggested that the probe could sensitively detect variations in HOCl level and viscosity in a dual-channel mode, and interference between the two channels can be neglected. Hence, the probe is applicable to detect AS progression more precisely using HOCl and viscosity as biomarkers simultaneously.

3.5. In vivo experiments of *AS-CN*

In view of the exciting success of the above results, we intended to exploit the probe for further the clinical application in *in vivo* AS detection. First, AS model was established in apolipoprotein E-deficient ($ApoE^{-/-}$) mice fed with a high-fat diet for 12 weeks, and C57BL/6 mice of the same sex and age were used as controls [42,43]. The right carotid artery ligation in mice at the 10th week of high-fat diet was carried out to strengthen the inflammation in the right carotid artery [44]. After

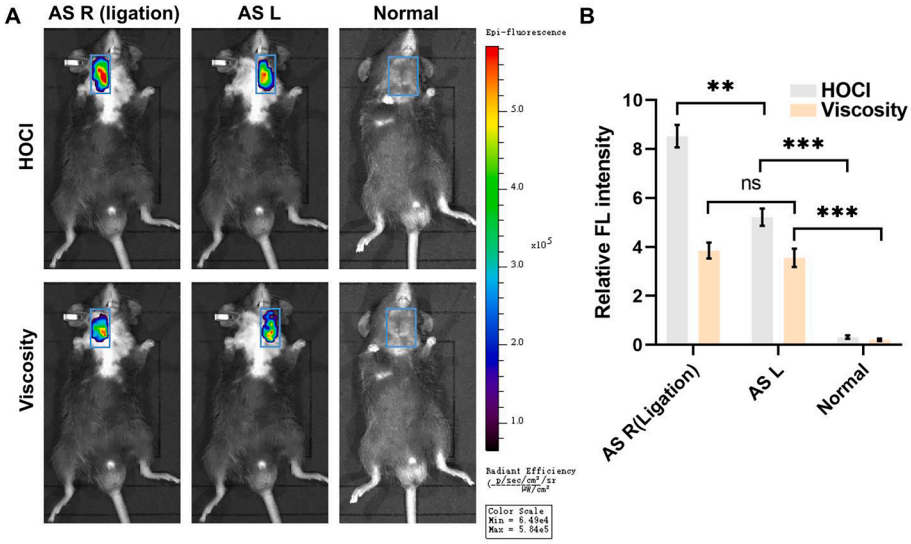

Fig. 7. Application of **AS-CN** in mice. (A) Noninvasive small animal *in vivo* fluorescence imaging of the left and right carotid arteries of the ligated AS mice and the carotid arteries of the healthy control group. (B) Average fluorescence intensity of **AS-CN** in fig. A. Data are mean ± SEM. ** $p < 0.01$, *** $p < 0.001$, ns: no statistical significance. Analyzed cells were obtained from three replicates. HOCl channel: $\lambda_{ex} = 430$ nm, $\lambda_{em} = 500–600$ nm; Viscosity channel: $\lambda_{ex} = 430$ nm, $\lambda_{em} = 690–790$ nm.

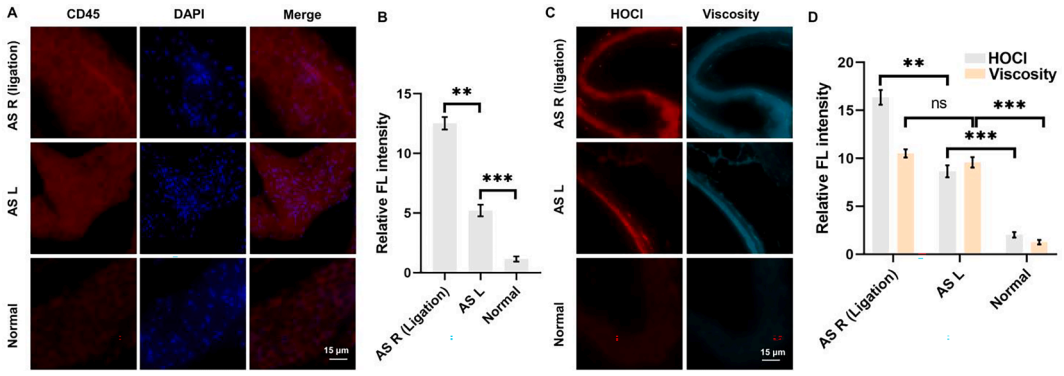

Fig. 8. (A) CD45 immunofluorescence staining of carotid artery sections and (B) the normalized average fluorescence intensity of CD45. (C) Fluorescent imaging of the HOCl (red) and viscosity (cyan) channels of **AS-CN** and (D) the normalized average fluorescence intensity of **AS-CN**. Data are mean ± SEM, $P < 0.05$ is considered significant. ** $p < 0.01$, *** $p < 0.001$, ns no statistical significance. Analyzed cells were obtained from three replicates. CD45 channel: $\lambda_{ex} = 561$ nm, $\lambda_{em} = 570–650$ nm; DAPI channel: $\lambda_{ex} = 364$ nm, $\lambda_{em} = 400–500$ nm HOCl channel: $\lambda_{ex} = 405$ nm, $\lambda_{em} = 500–600$ nm; Viscosity channel: $\lambda_{ex} = 445$ nm, $\lambda_{em} = 690–790$ nm. Scale bars on zoom images are 15 μm.

another 2 weeks of high-fat diet, the mice were injected with the probe **AS-CN** through the tail vein and imaged by a small animal *in vivo* imaging system after 60 min.

Before dual-channel imaging, the successful construction of the AS model in mice was verified by detected the blood lipid concentrations and Oil Red O staining (Fig. S13). Apparent lipid accumulation-induced obstruction in carotid artery sections was observed, suggesting the formation of AS. Afterwards, the fluorescence intensity from two channels of mouse carotid artery was collected. Compared with the control mice, the fluorescence intensity from HOCl channel was significantly enhanced in both of the right and left carotid arteries of ApoE$^{-/-}$ mice. Similar phenomena were visualized from viscosity channel (Fig. 7). Notably, as inflammation in the right carotid artery was amplified due to ligation, the HOCl level in there was obviously higher than that in the left carotid artery (Fig. 7B), suggesting HOCl level can reflect the degree of inflammation. By contrast, the viscosity in the bilateral carotid arteries kept almost the same.

In order to further explore the response otherness of HOCl and viscosity, tissue sections of the bilateral carotid arteries from mice in each group were acquired and subjected to immunofluorescence staining of CD45, a common marker of white blood [45]. As exhibited in Fig. 8A and B, on one hand, the expression of CD45 in the carotid arteries of ApoE$^{-/-}$ mice was obviously upregulated compared with that in normal ones, confirming the inflammation in AS mice. On the other hand, the expression of CD45 in the ligated right carotid artery is visibly higher than that in the left carotid artery, confirming the enhanced inflammation in the right carotid artery due to ligation. Meanwhile, the HOCl level and viscosity also increased in the atherosclerotic artery sections, and their variation tendencies were identical with the *in vivo* imaging results. Accordingly, the HOCl upregulation in ApoE$^{-/-}$ mice is tightly associated with CD45 expressions, i.e. the degree of inflammation, while viscosity as a physical variable might only respond to the lipid accumulation. It might be due to the fact that inflammation change is transient, while lipid accumulation is slowly progressed. In other words, ligation in the right carotid artery for 2 weeks apparently intensified its inflammation degree, but not promoted its lipid accumulation. As a result, we believe that HOCl and viscosity can act as the potential biomarkers for evaluating AS progression from different dimensions, i.e. chemical and physical, and the probe **AS-CN** serves as the first example for this purpose.

At present, anti-inflammatory therapy is opening up new ways to treat AS, yet it has not been formally accepted for clinical use [42,46]. Therefore, an efficient tool for assessing the treatment efficacy of anti-inflammatory drugs for AS treatment is of great significance. Thus, we attempted to utilize **AS-CN** to evaluate the efficacy of anti-inflammatory treatment in AS mice. Current research suggests that colchicine acts as an anti-inflammatory agent, and its anti-inflammatory activity for AS has been inspected in various clinical and experimental trials, which is likely to become a first-line treatment for AS and other cardiovascular inflammatory diseases in the future [47]. After 8 weeks of ApoE$^{-/-}$ mice on a high cholesterol diet, colchicine treatment (0.25 mg/kg body weight) was started once daily for more than four weeks [48], then imaging of the bilateral carotid arteries of AS mice was performed after injection with **AS-CN**. It should be noted that without ligation treatment, the approximate HOCl levels were recorded in the bilateral carotid arteries from ASmice. Moreover, there were no significant changes in the fluorescence intensities from the viscosity and HOCl channels between the colchicine-treated mice and the untreated AS mice (Fig. S14). This might be owing to the fact that a single anti-inflammatory treatment cannot effectively reduce the degree of AS. Anyway, this method can be used to indirectly evidence the treatment efficacy of colchicine in AS mice.

4. Conclusion

In summary, we propose a non-invasive detection approach using a dual-channel fluorescent probe **AS-CN**, to identify the degree of AS *in vivo* by detecting viscosity in a physical dimension and HOCl expression in a chemical dimension, respectively. Its fluorescence emission wavelength in response to viscosity is at 710 nm, and the fluorescence gradually increases with the increase of viscosity; the enhanced fluorescence response wavelength of HOCl is at 593 nm and has a superb sensitivity with the detection limit to be 12 nM. **AS-CN** not only has excellent performance in ordinary cell experiments, but also showcases feasibility for dynamically monitoring foam cell formation in two channels, which is extremely important for understanding underlying mechanism of atherosclerotic diseases at cellular level.

Declaration of Competing Interest

The authors declare that they have no known competing financial interests or personal relationships that could have appeared to influence the work reported in this paper.

Data availability

Data will be made available on request.

Acknowledgments

This work was supported by the National Natural Science Foundation of China (Nos. 22264013, 22207087, 22164009, and 21807029),

Hainan Province Science and Technology Special Fund (ZDYF2022SHFZ311), Natural Science Research Talent Project of Hainan Medical University (Grant JBGS202101), Key Laboratory of Clinical Laboratory Diagnosis and Translational Research of Zhejiang Province (Grant No: 2022E10022), Hainan Province Clinical Medical Center (2021), Project for Functional Materials and Molecular Imaging Science Innovation Group of Hainan Medical University.

Appendix A. Supplementary data

Supplementary data to this article can be found online at https://doi.org/10.1016/j.cej.2023.142687.

References

[1] S. Surma, M. Banach, Fibrinogen and atherosclerotic cardiovascular diseases-review of the literature and clinical studies, Int. J. Mol. Sci. 23 (1) (2021), https://doi.org/10.3390/ijms23010193.
[2] E. Ji, S. Lee, Antibody-based therapeutics for atherosclerosis and cardiovascular diseases, Int. J. Mol. Sci. 22 (11) (2021), https://doi.org/10.3390/ijms22115770.
[3] S.A. Ramsey, E.S. Gold, A. Aderem, A systems biology approach to understanding atherosclerosis, EMBO. Mol. Med. 2 (3) (2010) 79–89, https://doi.org/10.1002/emmm.201000063.
[4] J.F. Bentzon, F. Otsuka, R. Virmani, E. Falk, Mechanisms of plaque formation and rupture, Circ. Res. 114 (12) (2014) 1852–1866, https://doi.org/10.1161/CIRCRESAHA.114.302721.
[5] G. Fredman, K.C. MacNamara, Atherosclerosis is a major human killer and non-resolving inflammation is a prime suspect, Cardiovasc. Rese. 117 (13) (2021) 2563–2574, https://doi.org/10.1093/cvr/cvab309.
[6] J.L.M. Bjorkegren, A.J. Lusis, Atherosclerosis: recent developments, Cell 185 (10) (2022) 1630–1645, https://doi.org/10.1016/j.cell.2022.04.004.
[7] J. Chen, X. Zhang, R. Millican, J. Sherwood, S. Martin, H. Jo, Y.S. Yoon, B.C. Brott, H.W. Jun, Recent advances in nanomaterials for therapy and diagnosis for atherosclerosis, Adv. Drug. Deliv. Rev. 170 (2021) 142–199, https://doi.org/10.1016/j.addr.2021.01.005.
[8] X. Feng, L. Zhang, S. Xu, A.Z. Shen, ATP-citrate lyase (ACLY) in lipid metabolism and atherosclerosis: an updated review, Prog. Lipid. Res. 77 (2020) 101006, https://doi.org/10.1016/j.plipres.2019.101006.
[9] S. Zhang, L. Li, W. Chen, S. Xu, X. Feng, L. Zhang, Natural products: the role and mechanism in low-density lipoprotein oxidation and atherosclerosis, Phytother. Res. 35 (6) (2021) 2945–2967, https://doi.org/10.1002/ptr.7002.
[10] G.D. Sloop, D.W. Garber, The effects of low-density lipoprotein and high-density lipoprotein on blood viscosity correlate with their association with risk of atherosclerosis in humans, Clin. Sci. 92 (5) (1997) 473–479, https://doi.org/10.1042/cs0920473.
[11] A. Gistera, G.K. Hansson, The immunology of atherosclerosis, Nat. Rev. Nephrol. 13 (6) (2017) 368–380, https://doi.org/10.1038/nrneph.2017.51.
[12] E.M. Maguire, S.W.A. Pearce, Q. Xiao, Foam cell formation: a new target for fighting atherosclerosis and cardiovascular disease, Vascul. Pharmacol. 112 (2019) 54–71, https://doi.org/10.1016/j.vph.2018.08.002.
[13] P. Marchio, S. Guerra-Ojeda, J.M. Vila, M. Aldasoro, V.M. Victor, M.D. Mauricio, Targeting early atherosclerosis: a focus on oxidative stress and inflammation, Oxid. Med. Cell. Longev. 2019 (2019) 8563845, https://doi.org/10.1155/2019/8563845.
[14] S.D. Stojanovic, J. Fiedler, J. Bauersachs, T. Thum, D.G. Sedding, Senescence-induced inflammation: an important player and key therapeutic target in atherosclerosis, Eur. Heart. J. 41 (31) (2020) 2983–2996, https://doi.org/10.1093/eurheartj/ehz919.
[15] X. Feng, W. Chen, X. Ni, P.J. Little, S. Xu, L. Tang, J. Weng, Metformin, macrophage dysfunction and atherosclerosis, Front. Immunol. 12 (2021) 682853, https://doi.org/10.3389/fimmu.2021.682853.
[16] T. Shemiakova, E. Ivanova, W.-K. Wu, T.V. Kirichenko, A.V. Starodubova, A. N. Orekhov, Atherosclerosis as mitochondriopathy: repositioning the disease to help finding new therapies, Front. Cardiovasc. Med. 8 (2021), https://doi.org/10.3389/fcvm.2021.660473.
[17] V.M. Victor, N. Apostolova, R. Herance, A. Hernandez-Mijares, M. Rocha, Oxidative stress and mitochondrial dysfunction in atherosclerosis: mitochondria-targeted antioxidants as potential therapy, Curr. Med. Chem. 16 (35) (2009) 4654–4667, https://doi.org/10.2174/092986709789878265.
[18] J.T. Hou, B. Wang, Y. Zou, P. Fan, X. Chang, X. Cao, S. Wang, F. Yu, Molecular fluorescent probes for imaging and evaluation of hypochlorite fluctuations during diagnosis and therapy of osteoarthritis in cells and in a mouse model, ACS. Sens. 5 (7) (2020) 1949–1958, https://doi.org/10.1021/acssensors.0c00270.
[19] Y. Huang, W. Chen, J. Chung, J. Yin, J. Yoon, Recent progress in fluorescent probes for bacteria, Chem. Soc. Rev. 50 (13) (2021) 7725–7744, https://doi.org/10.1039/d0cs01340d.
[20] S. Wang, W.X. Ren, J.T. Hou, M. Won, J. An, X. Chen, J. Shu, J.S. Kim, Fluorescence imaging of pathophysiological microenvironments, Chem. Soc. Rev. 50 (16) (2021) 8887–8902, https://doi.org/10.1039/d1cs00083g.
[21] A. Aliyan, N.P. Cook, A.A. Marti, Interrogating amyloid aggregates using fluorescent probes, Chem. Rev. 119 (23) (2019) 11819–11856, https://doi.org/10.1021/acs.chemrev.9b00404.
[22] D. Cheng, W. Xu, X. Gong, L. Yuan, X.B. Zhang, Design strategy of fluorescent probes for live drug-induced acute liver injury imaging, Acc. Chem. Res. 54 (2) (2021) 403–415, https://doi.org/10.1021/acs.accounts.0c00646.
[23] D. Cheng, Y. Pan, L. Wang, Z. Zeng, L. Yuan, X. Zhang, Y.T. Chang, Selective visualization of the endogenous peroxynitrite in an inflamed mouse model by a mitochondria-targetable two-photon ratiometric fluorescent probe, J. Am. Chem. Soc. 139 (1) (2017) 285–292, https://doi.org/10.1021/jacs.6b10508.
[24] D. Wu, A.C. Sedgwick, T. Gunnlaugsson, E.U. Akkaya, J. Yoon, T.D. James, Fluorescent chemosensors: the past, present and future, Chem. Soc. Rev. 46 (23) (2017) 7105–7123, https://doi.org/10.1039/c7cs00240h.
[25] J. Li, K. Wang, W. Pan, N. Li, B. Tang, Targeted imaging in atherosclerosis, Anal. Chem. 94 (36) (2022) 12263–12273, https://doi.org/10.1021/acs.analchem.2c02644.
[26] J. Li, N. Zhao, W. Zhang, P. Li, X. Yin, W. Zhang, H. Wang, B. Tang, Assessing the progression of early atherosclerosis mice using a fluorescence nanosensor for the simultaneous detection and imaging of pH and phosphorylation, Angew. Chem. Int. Ed. Engl. 62 (3) (2023) e202215178.
[27] Z. Ye, M. Ji, K. Wu, J. Yang, A.A. Liu, W. Sun, D. Ding, D. Liu, In-sequence high-specificity dual-reporter unlocking of fluorescent probe enables the precise identification of atherosclerotic plaques, Angew. Chem. Int. Ed. Engl. 61 (29) (2022) e202204518.
[28] C.M. Li, W.H. Zhuang, Y.C. Wang, S.F. Li, J.R. Chen, L.S. Zhou, Y.B. Liao, M. Chen, J.S. You, Specific lipid droplet imaging of atherosclerotic plaques and fatty liver using an imidazole-based fluorescence probe, Dyes. Pigm. 204 (2022). https://doi.org/ARTN 11043910.1016/j.dyepig.2022.110439.
[29] J.R. Zheng, S.H. Qin, L.J. Gui, H. Li, L.X. Fan, Y.F. Yang, H.Y. Chen, H. Xu, Z. W. Yuan, Light-up lipid droplets for the visualization of lipophagy and atherosclerosis by coumarin-derived bioprobe, Chin. Chem. Lett. 32 (8) (2021) 2385–2389, https://doi.org/10.1016/j.cclet.2021.02.059.
[30] M.K. Cho, M.J. Seo, V. Juvekar, J.H. Jo, W. Kim, K.S. Choi, H.M. Kim, Screening of drug-induced steatosis and phospholipidosis using lipid droplet-selective two-photon probes, Anal. Chem. 92 (16) (2020) 11223–11231, https://doi.org/10.1021/acs.analchem.0c01728.
[31] M.M. Zhang, Y.H. Ma, P. Li, Y. Jia, K.L. Han, Detection of atherosclerosis-related hypochlorous acid produced in foam cells with a localized endoplasmic reticulum probe, Chem. Commun. 56 (17) (2020) 2610–2613, https://doi.org/10.1039/d0cc00090f.
[32] B.Y. Wang, F.Y. Yuan, S. Wang, R. Duan, W.X. Ren, J.T. Hou, Detection of atherosclerosis-associated HOCl using a mitochondria-targeted fluorescent probe, Sensor. Actuat. B-Chemical. 348 (2021). https://doi.org/ARTN 13069510.1016/j.snb.2021.130695.
[33] J.T. Hou, K.K. Yu, K. Sunwoo, W.Y. Kim, S. Koo, J.Y. Wang, W.X. Ren, S. Wang, X. Q. Yu, J.S. Kim, Fluorescent imaging of reactive oxygen and nitrogen species associated with pathophysiological processes, Chem-Us. 6 (4) (2020) 832–866, https://doi.org/10.1016/j.chempr.2019.12.005.
[34] Y. Ma, Y. Zhao, R. Guo, L. Zhu, W. Lin, A near-infrared emission fluorescent probe with multi-rotatable moieties for highly sensitive detection of mitochondrial viscosity in an inflammatory cell model, J. Mater. Chem. B. 6 (39) (2018) 6212–6216, https://doi.org/10.1039/c8tb02083c.
[35] J.T. Hou, N. Kwon, S. Wang, B.Y. Wang, X.J. He, J. Yoon, J.L. Shen, Sulfur-based fluorescent probes for HOCl: mechanisms, design, and applications, Coord. Chem. Rev. 450 (2022). https://doi.org/ARTN 21423210.1016/j.ccr.2021.214232.
[36] G.L. Niu, R.Y. Zhang, J.P.C. Kwong, J.W.Y. Lam, C.P. Chen, J.G. Wang, Y.C. Chen, X. Feng, R.T.K. Kwok, H.H.Y. Sung, I.D. Williams, M.R.J. Elsegood, J.N. Qu, C. Ma, K.S. Wong, X.Q. Yu, B.Z. Tang, Specific two-photon imaging of live cellular and deep-tissue lipid droplets by lipophilic aiegens at ultralow concentration, Chem. Mater. 30 (14) (2018) 4778–4787, https://doi.org/10.1021/acs.chemmater.8b01943.
[37] L. Yu, J.F. Zhang, M.L. Li, D.W. Jiang, Y. Zhou, P. Verwilst, J.S. Kim, Combining viscosity-restricted intramolecular motion and mitochondrial targeting leads to selective tumor visualization, Chem. Commun. 56 (49) (2020) 6684–6687, https://doi.org/10.1039/d0cc02943b.
[38] D.D. Su, C.L. Teoh, L. Wang, X.G. Liu, Y.T. Chang, Motion-induced change in emission (MICE) for developing fluorescent probes, Chem. Soc. Rev. 46 (16) (2017) 4833–4844, https://doi.org/10.1039/c7cs00018a.
[39] X. Tian, L.C. Murfin, L. Wu, S.E. Lewis, T.D. James, Fluorescent small organic probes for biosensing, Chem. Sci. 12 (10) (2021) 3406–3426, https://doi.org/10.1039/d0sc06928k.
[40] G. Ferrer-Sueta, R. Radi, Chemical biology of peroxynitrite: kinetics, diffusion, and radicals, ACS. Chem. Biol. 4 (3) (2009) 161–177, https://doi.org/10.1021/cb800279q.
[41] A. Zheng, H. Liu, X. Gao, K. Xu, B. Tang, A mitochondrial-targeting near-infrared fluorescent probe for revealing the effects of hydrogen peroxide and heavy metal ions on viscosity, Anal. Chem. 93 (26) (2021) 9244–9249, https://doi.org/10.1021/acs.analchem.1c01511.
[42] X. T. Li, J. Y. Gu, Q.Q. Xiao, Y. Liu, P. Zhou, L.F. Fan, X.L. Zhang, X. Lu, J. Wu, Z.X. Liu, W. He, Liposomal codelivery of inflammation inhibitor and collagen protector to the plaque for effective anti-atherosclerosis, Chin. Chem. Lett. 34(1) (2023). https://doi.org/ARTN 10748310.1016/j.cclet.2022.04.081.
[43] Y. Zhao, H. Qu, Y. Wang, W. Xiao, Y. Zhang, D. Shi, Small rodent models of atherosclerosis, Biomed. Pharmacother. 129 (2020) 110426, https://doi.org/10.1016/j.biopha.2020.110426.
[44] N.P. Withana, T. Saito, X.W. Ma, M. Garland, C.H. Liu, H. Kosuge, M. Amsallem, M. Verdoes, L.O. Ofori, M. Fischbein, M. Arakawa, Z. Cheng, M.V. McConnell, M. Bogyo, Dual-modality activity-based probes as molecular imaging agents for

vascular inflammation, J. Nucl. Med. 57 (10) (2016) 1583–1590, https://doi.org/10.2967/jnumed.115.171553.
[45] M.L. Vlad, S.A. Manea, A.G. Lazar, M. Raicu, H. Muresian, M. Simionescu, A. Manea, Histone acetyltransferase-dependent pathways mediate upregulation of NADPH oxidase 5 in human macrophages under inflammatory conditions: a potential mechanism of reactive oxygen species overproduction in atherosclerosis, Oxid. Med. Cell. Longev. 2019 (2019) 3201062, https://doi.org/10.1155/2019/3201062.
[46] Y.L. Song, H.Q. Jing, L.B. Vong, J.P. Wang, N. Li, Recent advances in targeted stimuli-responsive nano-based drug delivery systems combating atherosclerosis, Chin. Chem. Lett. 33 (4) (2022) 1705–1717, https://doi.org/10.1016/j.cclet.2021.10.055.
[47] P. Libby, Inflammation in atherosclerosis-no longer a theory, Clin. Chem. 67 (1) (2021) 131–142, https://doi.org/10.1093/clinchem/hvaa275.
[48] U. Meyer-Lindemann, C. Mauersberger, A.C. Schmidt, A. Moggio, J. Hinterdobler, X. Li, D. Khangholi, J. Hettwer, C. Grasser, A. Dutsch, H. Schunkert, T. Kessler, H. B. Sager, Colchicine impacts leukocyte trafficking in atherosclerosis and reduces vascular inflammation, Front. Immunol. 13 (2022) 898690, https://doi.org/10.3389/fimmu.2022.898690.